Second harmonic generation in nano-structured thin-film lithium niobate waveguides

Cheng Wang,[1,†] Xiao Xiong,[1,2,†] Nicolas Andrade,[1,3] Vivek Venkataraman,[1] Xi-Feng Ren,[2] Guang-Can Guo,[2] and Marko Lončar[1,*]

1John A. Paulson School of Engineering and Applied Sciences, Harvard University, 29 Oxford Street, Cambridge, MA 02138, USA
[2]Key Laboratory of Quantum Information & Synergetic Innovation Center of Quantum Information & Quantum Physics, University of Science and Technology of China, Hefei, Anhui 230026, China
[3]Department of Electrical and Computer Engineering, Virginia Commonwealth University, Richmond, Virginia 23284, USA
**Corresponding author: loncar@seas.harvard.edu*

Lithium niobate is the most well-known optical material with a second-order $\chi^{(2)}$ nonlinearity that is widely employed in modern optical technology. Integrated lithium niobate platform has recently emerged as a promising candidate for next-generation, high-efficiency wavelength conversion systems that allow dense packaging and mass-production. Here we demonstrate efficient, phase-matched second harmonic generation in lithographically-defined thin-film lithium niobate waveguides with sub-micron dimensions. Both natural phase matching in fixed-width waveguides and quasi-phase matching in periodically-grooved waveguides are theoretically proposed and experimentally demonstrated. Our low-loss (~2.52 dB/cm) nanowaveguides possess normalized conversion efficiencies as high as 41% $W^{-1}cm^{-2}$, promising for future on-chip quantum wavelength conversion.

1. INTRODUCTION

Second order ($\chi^{(2)}$) nonlinear optical processes, including second harmonic generation (SHG), sum/difference frequency generation (SFG/DFG), and parametric down conversion, not only are crucial for accessing new spectral ranges in classical optics [1-3], but also act as key resources for non-classical light generation in quantum information processing [4-6]. Conventional second order wavelength conversion systems are mostly realized in ion-exchanged periodically poled lithium niobate (PPLN) waveguides, where quasi-phase matching is achieved by periodic domain inversion [7-11]. These devices take advantage of lithium niobate's ($LiNbO_3$, LN) large diagonal $\chi^{(2)}$ coefficient (d_{33} = 27 pm/V) and wide transmission window from UV to mid-IR [12]. However, the low index contrast ($\Delta n \sim 0.02$) between waveguide core and cladding usually results in large device dimensions (~ cm long and ~ 10 μm wide) and large bending radii (mm scale) [13], preventing dense integration.

On the other hand, recent years have seen tremendous progress in the field of nonlinear nanophotonics [14-22]. Nonlinear interactions could be enhanced by orders of magnitude due to the superior light confinement in these wavelength-scale devices. Moreover, the use of well-developed nanofabrication methods offers the possibility to build scalable, low-cost and highly integrated nonlinear optical systems.

While LN's linear and nonlinear optical properties offer unique opportunities for novel devices, realization of LN nanophotonics has remained challenging until the recent commercial availability of LN on insulator (LNOI) substrates and development on LN nanofabrication techniques [23]. Since then, various thin-film LN optical components have been realized, including microdisk resonators [24-26], microring resonators [27, 28], photonic crystals [29], and low-loss waveguides [30, 31].

In this work we demonstrate efficient SHG in low-loss (~2.52dB/cm) thin-film LN nanowaveguides, with normalized conversion efficiencies as high as 41% $W^{-1}cm^{-2}$. This is enabled by the ability to precisely engineer the dispersion properties and device dimensions of the LN nanowaveguides by the top-down fabrication method we use. To achieve the phase matching condition in our devices, we theoretically propose and experimentally demonstrate two distinct schemes: (1) natural phase matching between 1st and 3rd order transverse-electric (TE) modes in waveguides of fixed width; (2) quasi-phase matching in periodically grooved lithium niobate (PGLN) waveguides. We show that both methods feature unique advantages and are promising for on-chip quantum nonlinear wavelength conversion.

2. DESIGN AND SIMULATIONS

Figure 1(a) displays the cross-section schematic of a typical x-cut thin-film LNOI waveguide cladded in silica. The geometric parameters of such a waveguide include top width w_t, bottom width w_b, thickness t, and sidewall angle θ (introduced by the dry etching process). The coordinates in Fig. 1(a) are aligned with the crystalline directions of LN, where z is the extraordinary axis. This waveguide geometry supports both TE like and transverse-magnetic (TM) like modes. However, here we are interested in the TE modes only in order to access the largest nonlinear coefficient (d_{33} = 27 pm/V) [12]. Figure 1(b) shows the dependence of effective mode indices (n_{eff}) of both fundamental mode at pump wavelength (~ 1550 nm) as well as fundamental and higher order modes at second harmonic (SH) wavelength (~ 775 nm) as a function of waveguide top width (w_t). Representative modal profiles at both wavelengths are displayed in Fig. 1(c). The results were obtained using a Finite Difference Eigenmode solver (MODE Solutions, Lumerical). In the simulation, we use t = 400 nm and θ = 40°, which are taken from actual device dimensions. To achieve phase matching, n_{eff} at both wavelengths need to be equal. In our system this cannot be achieved for fundamental TE modes at pump and SH wavelengths, due to both material and waveguide dispersions. In the following sections, we show two methods to address the phase mismatch issue based on the waveguide dispersion displayed in Fig. 1(b).

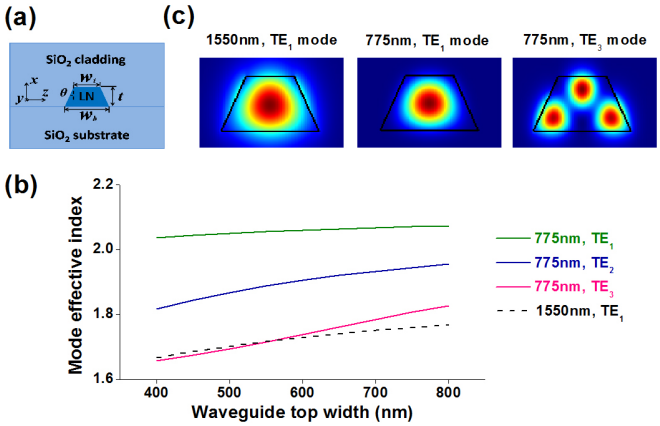

Fig. 1. (a) Cross-section schematic of the x-cut LNOI waveguide, where the coordinates are aligned with the LN crystal directions. (b) Mode effective indices as a function of waveguide top width at both pump and SH wavelengths. (c) Corresponding modal profile at both wavelengths.

A. Natural phase matching between 1st and 3rd order TE modes

To achieve natural phase matching, higher order modes at SH wavelength can be used to bring down the n_{eff} to match with that of the fundamental mode at pump wavelength. Note that conversion between TE_1 mode at fundamental wavelength and TE_2 mode at SH wavelength is prohibited by symmetry. Therefore the lowest possible phase-matching mode at SH wavelength is TE_3. In fact, Fig. 1 (b) suggests that phase matching is readily achievable with $w_t \sim 580$ nm.

Using the slowly-varying envelope approximation, we can express the electric field inside a waveguide as:

$$\mathbb{E}^q(x,y,z) = a^q(y)E^q(x,z)exp(-j\beta^q y) \quad (1)$$

where $a^q(y)$is the field amplitude envelope that varies slowly along the y-axis, $E^q(x,z)$is the normalized electric field distribution in the waveguide cross section, and β is the propagation constant. $q \in \{\omega, 2\omega\}$ represents the corresponding optical frequencies. Substituting Eq. (1) into Maxwell's equations, we obtain:

$$\frac{d}{dy}a^q(y) = -j\frac{\omega}{4}\iint (E^q(x,z))^* exp(j\beta^q y)P^q dxdz \quad (2)$$

where P^q is the nonlinear polarization, written as:

$$P^{\omega} = 2d_{33}E^{2\omega}E^{\omega *},\ P^{2\omega} = d_{33}E^{\omega}E^{\omega} \quad (3)$$

Substituting Eq. (3) into Eq. (2), the nonlinear coupled-mode equations can be written as:

$$\frac{d}{dy}a^{\omega}(y) = -j2g^* a^{2\omega}(y)a^{\omega *}(y)exp(-j\delta y) \quad (4)$$

$$\frac{d}{dy}a^{2\omega}(y) = -jg(a^{\omega}(y))^2 exp(j\delta y) \quad (5)$$

where $\delta = \beta^{2\omega} - 2\beta^{\omega}$ is the phase mismatch, and the overlap factor g is given by:

$$g = \frac{\omega}{4}\iint (E^{2\omega}(x,z))^* d_{33}(x,z)(E^{\omega}(x,z))^2 dxdz \quad (6)$$

In the low-conversion limit, the SHG conversion efficiency in a waveguide can be solved as:

$$\gamma = \frac{|a^{2\omega}(L)|^2}{|a^{\omega}(0)|^2} = g^2 L^2 P_0 (\frac{sin(\delta L/2)}{\delta L/2})^2 \quad (7)$$

where L is the waveguide length, P_0 is the input optical power.

Note that, Eq. (7) has the same form as SHG in a bulk nonlinear crystal, except for the overlap factor g. Considering the natural phase matching case ($\delta = 0$), the normalized (by length and input power) conversion efficiency η is simply g^2.

Using practical waveguide parameters (w_t = 600 nm, w_b = 1270 nm, t = 400 nm), and mode profiles for fundamental pump and third order SH mode, we obtain a nonlinear overlap factor g = 0.774 $W^{-1/2}cm^{-1}$, which corresponds to a normalized conversion efficiency η of 59.9% $W^{-1}cm^{-2}$.

B. Periodically-grooved lithium niobate (PGLN) waveguides

In conventional nonlinear optics, quasi-phase matching is realized by periodically inverting the ferroelectric crystal direction [32]. Here, we utilize a periodically-grooved structure to achieve quasi-phase matching between fundamental TE modes at both pump and SH wavelengths. By introducing periodic modulation of the waveguide width, as shown in Fig. 2(a), with a period Λ, an additional momentum "kick" $\Delta k = 2\pi/\Lambda$ could be applied to the propagating electromagnetic wave, compensating for the phase mismatch δ.

To analytically solve the nonlinear coupled-mode equations in this case, we consider the PGLN waveguide as a perturbation from the uniform waveguide case (described in Section 2A), with both the linear permittivity ε and nonlinear coefficient d_{33} periodically modulated along the propagation direction (y-axis). We can therefore expand both $\Delta\varepsilon$ (permittivity difference between waveguide and environment) and d_{33} as Fourier series in y:

$$\Delta\varepsilon(x,y,z) = \sum_m \Delta\varepsilon_m(x,z)exp(-jm\Delta ky) \quad (8)$$

$$d_{33}(x,y,z) = \sum_m d_{33}^{(m)}(x,z)exp(-jm\Delta ky) \quad (9)$$

In this case, the polarization term in Eq. (2) consists of both linear and nonlinear components, written as:

$$P^{\omega} = \varepsilon_0\Delta\varepsilon^{\omega}E^{\omega} + 2d_{33}E^{2\omega}E^{\omega *} \quad (10)$$

$$P^{2\omega} = \varepsilon_0\Delta\varepsilon^{2\omega}E^{2\omega} + d_{33}E^{\omega}E^{\omega} \quad (11)$$

By substituting Eqs. (8)-(11) into Eq. (2), the nonlinear coupled-mode equations can be written as:

$$\frac{d}{dy}a^{\omega}(y) + j\left[2g_L^{\omega}cos(\theta(y))\right]a^{\omega}(y) = -j\sum_m [g_{NL}^{(m)}exp\left(j\delta_m{}'(y)\right)]^*(a^{\omega}(y))^* a^{2\omega}(y) \quad (12)$$

$$\frac{d}{dy}a^{2\omega}(y) + j\left[2g_L^{2\omega}cos(\theta(y))\right]a^{2\omega}(y) = -j\sum_m [g_{NL}^{(m)}exp\left(j\delta_m{}'(y)\right)](a^{\omega}(y))^2 \quad (13)$$

with

$$g_{NL}^{(m)} = \frac{2\omega}{4}\iint (E^{2\omega}(x,z))^* d_{33}^{(m)}(x,z)(E^{\omega}(x,z))^2 dxdz \quad (14)$$

$$g_L^{\omega} = \frac{\omega\varepsilon_0}{4}\iint \Delta\varepsilon_1^{\omega}(x,z)|E^{\omega}(x,z)|^2 dxdz \quad (15)$$

$$g_L^{2\omega} = \frac{2\omega\varepsilon_0}{4}\iint \Delta\varepsilon_1^{2\omega}(x,z)|E^{2\omega}(x,z)|^2 dxdz \quad (16)$$

Replace a^{ω} and $a^{2\omega}$ with:

$$a^{\omega}(y) = A^{\omega}(y)exp\ [-j(2g_L^{\omega}/\Delta k)sin\ (\Delta ky)] \quad (17)$$

$$a^{2\omega}(y) = A^{2\omega}(y)exp\ [-j(2g_L^{2\omega}/\Delta k)sin\ (\Delta ky)] \quad (18)$$

and use $\sum_p J_p(\vartheta)exp(jp\Delta ky) = exp[j\vartheta sin(\Delta ky)]$, we get the new coupled-mode equations:

$$\frac{d}{dy}A^{\omega}(y) = -jg'^* A^{2\omega}(y)(A^{\omega}(y))^* exp(-j\delta' y) \quad (19)$$

$$\frac{d}{dy}A^{2\omega}(y) = -jg'\left(A^{\omega}(y)\right)^2 exp(j\delta' y) \quad (20)$$

Comparing with Eqs. (4)-(5), here the phase mismatch term becomes $\delta' = \beta^{2\omega} - 2\beta^{\omega} - 2\pi/\Lambda$, and the new overlap factor $g'$is expressed as:

$$g' = g_{NL}^{(1)}(J_0(\varphi_L) + J_2(\varphi_L)) - g_{NL}^{(0)}J_1(\varphi_L) \quad (21)$$

where J_p denotes the p-th order Bessel function (only first three terms with slow spatial variation are taken), and

$$\varphi_L = 2(g_L^{2\omega} - 2g_L^{\omega})/\Delta k \quad (22)$$

The new overlap factor g'consists of two terms. The first term results from the periodically varying nonlinear coefficient $d_{33}^{(1)}$, which is the same effect as in PPLN. The second term originates from the constant nonlinear coefficient $d_{33}^{(0)}$ and periodically modulated dielectric constant $\Delta\varepsilon_1$, or grating effect. Details of the PGLN theory can be found in Ref. [33].

For a typical PGLN waveguide (w_t = 670 nm, w_b = 1300 nm, t = 400 nm) with a periodic groove depth of 80 nm, the nonlinear coupling coefficient is calculated to be g' = 0.345 $W^{-1/2}cm^{-1}$, which corresponds to a normalized conversion efficiency η of 12.1% $W^{-1}cm^{-2}$. The total conversion efficiency η in the low-conversion limit is plotted as a function of propagation length in Fig. 2(b), in comparison with a uniform waveguide without periodic grooves. Here we also take into consideration the oscillating phase-mismatched optical fields, which could be obtained simply by replacing the overlap factor in Eqs. (19)-(20) with $G' = g' + g_{NL}^{(0)}J_0(\varphi_L)exp\ (j\Delta ky)$. The net conversion

efficiency features a quadratically increasing envelope with local oscillations.

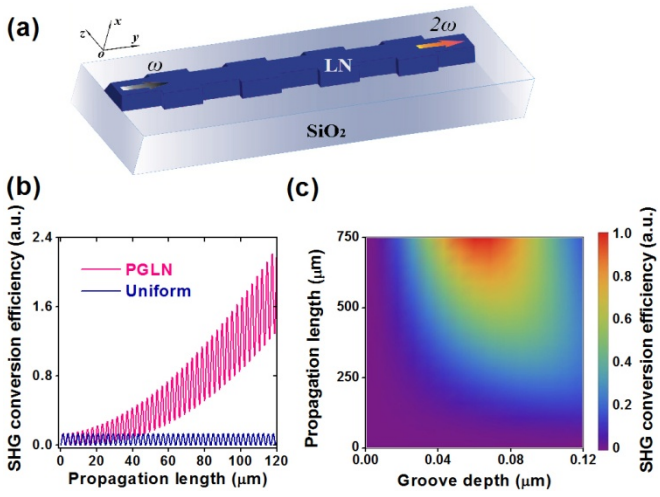

Fig. 2. (a) 3D cartoon of the proposed PGLN structure. (b) Simulated SHG efficiencies versus propagation length for a PGLN waveguide with a groove depth of 80 nm, in comparison with a uniform LN waveguide. (c) SHG efficiency dependence on groove depth and propagation length, showing the trade-off between the nonlinear overlap and scattering loss.

In a realistic PGLN waveguide, the waveguide scattering loss due to the periodic grooves is not negligible. In fact, while a larger groove depth enhances the nonlinear overlap g', it also induces more scattering loss. In order to model this trade-off, we introduce two loss terms in the nonlinear coupled-mode equations. Assuming that the pump is not depleted by the generated SH, the coupled-mode equations can be rewritten as:

$$\frac{d}{dy}A^{\omega}(y) = -\alpha^{\omega}A^{\omega}(y) \quad (23)$$

$$\frac{d}{dy}A^{2\omega}(y) = -jg'(A^{\omega}(y))^2 exp(j\delta' y) - \alpha^{2\omega}A^{2\omega}(y) \quad (24)$$

where α^{ω}, $\alpha^{2\omega}$ are the loss coefficients of the PGLN waveguide for pump and SH wavelengths respectively, calculated using the Finite Difference Time Domain method (FDTD Solutions, Lumercial).

In the case that the groove period exactly compensates for the initial phase mismatch, or $\delta' = 0$, the new conversion efficiency including the waveguide loss can be expresses as:

$$\gamma' = \frac{|A^{2\omega}(L)|^2}{|A^{\omega}(0)|^2} = g'^2 P_0 \left(\frac{exp(-2\alpha^{\omega}L) - exp(-\alpha^{2\omega}L)}{2\alpha^{\omega} - \alpha^{2\omega}}\right)^2 \quad (25)$$

Figure 2(c) shows the theoretical result of conversion efficiency as a function of groove depth and waveguide length. The optimal groove depth is smaller for a longer PGLN waveguide to limit the total loss to a reasonable value. For a waveguide length of 500 μm used in the following experiments, the optimal groove depth is ~ 80 nm.

3. DEVICE FABRICATION

Starting from an x-cut LNOI substrate (400 nm thick, NANOLN), uniform and PGLN waveguides were fabricated using a process modified from Ref. [24]. An amorphous silicon layer (a-Si, 800 nm thick) was first deposited on the substrate via plasma-enhanced chemical vapor deposition (PECVD). The a-Si layer was then patterned with a combination of electron-beam lithography (EBL) and reactive ion etching (RIE), and used as a hard mask for the subsequent LN dry etching in Ar^+ plasma. After removing leftover silicon mask in KOH (80 °C), the waveguides were cladded in silica using PECVD. Waveguide facets were diced and polished to ensure high coupling efficiency. Figure 3 shows the scanning electron microscope (SEM) images of uniform LN and PGLN waveguides without cladding. It can be seen that our fabrication process is well capable of delivering designed structures, while maintaining minimum surface roughness and manageable scattering loss.

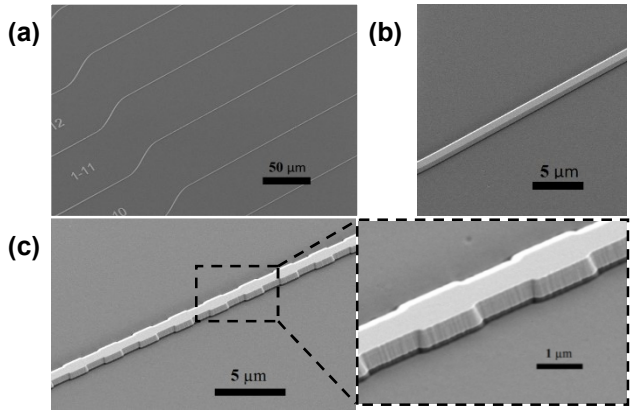

Fig. 3. Representative scanning electron microscope images of the fabricated devices. (a) An array of LN waveguides with slightly different widths. (b) A typical uniform LN waveguide with fixed width. (c) A typical PGLN waveguide with a spatial modulation period of 2.77 μm and a groove depth of 80 nm.

4. OPTICAL MEASUREMENTS

We measured the SHG response of both naturally phase-matched LN and PGLN waveguides using the setup shown in Fig. 4(a). Tunable telecom lasers (Santec TSL-510, 1480 – 1680 nm) were used as light sources at pump wavelength. A fiber polarization controller was used to ensure TE mode input before end-fire coupling into the device under test. Light is coupled into and out of the waveguide facets using tapered lensed fibers. The output light is sent to either an InGaAs photodetector, or a silicon avalanche photodetector (APD), to monitor the linearly transmitted telecom light and the SHG signal respectively.

Figure 4(b) shows the linear transmission spectrum (in absolute unit) of a typical uniform waveguide at telecom wavelengths. It indicates a total fiber-to-fiber loss ~ 7.45 dB, resulting from a combination of facet coupling loss and waveguide propagation loss. The fringe pattern seen in Fig. 4(b) is a result of Fabry-Perot interference between the two polished facets of the waveguide. From the contrast between maximum and minimum of the transmission fringes, we can extract the waveguide propagation loss using the following equation [34]:

$$\alpha = \frac{4.34}{L}\left(lnR - ln\tilde{R}\right) \quad (26)$$

with $\tilde{R} = \frac{1}{K}\left(1 - \sqrt{1-K^2}\right)$, $K = \frac{I_{max}-I_{min}}{I_{max}+I_{min}}$. Here I_{max} and I_{min} are the maximum and minimum intensities of the transmitted light. R is the reflection coefficient at the waveguide facet, which is calculated to be 0.147 using FDTD. L is the waveguide length, which is 3 mm in this case. The waveguide propagation loss is thus calculated to be 2.52 dB/cm. This value represents the best propagation loss reported in thin-film LN waveguides with sub-wavelength light confinement (A_{eff} = 0.52 μm² at telecom wavelength), and is consistent with the quality factor achieved in our previous microdisk resonators [24]. Using the calculated propagation loss and the measured transmission, we are able to estimate the fiber-to-waveguide coupling efficiency. By characterizing many waveguides on the same chip used in the following experiments, an average coupling efficiency of (25 ± 5)% on each facet is extracted.

Figures 4(c) and 4(d) show the measured SHG efficiencies as a function of SH wavelength for both naturally phase matched LN waveguides (1 mm long) and quasi-phase matched PGLN waveguides (0.5 mm long). These values have accounted for the APD spectral quantum efficiency and the facet coupling loss, and are normalized by the pump laser power. For each scheme, a set of waveguides with slightly different widths are characterized. SHG peaks can be clearly observed at the corresponding (quasi-) phase matching wavelengths. The SHG peak wavelength changes with increasing waveguide width in both cases, but in opposite directions, which agrees with theoretical prediction. When normalized by waveguide length, the SH conversion

efficiencies for naturally phase matched and quasi-phase matched cases are 41% $W^{-1}cm^{-2}$ and 7.0% $W^{-1}cm^{-2}$, respectively.

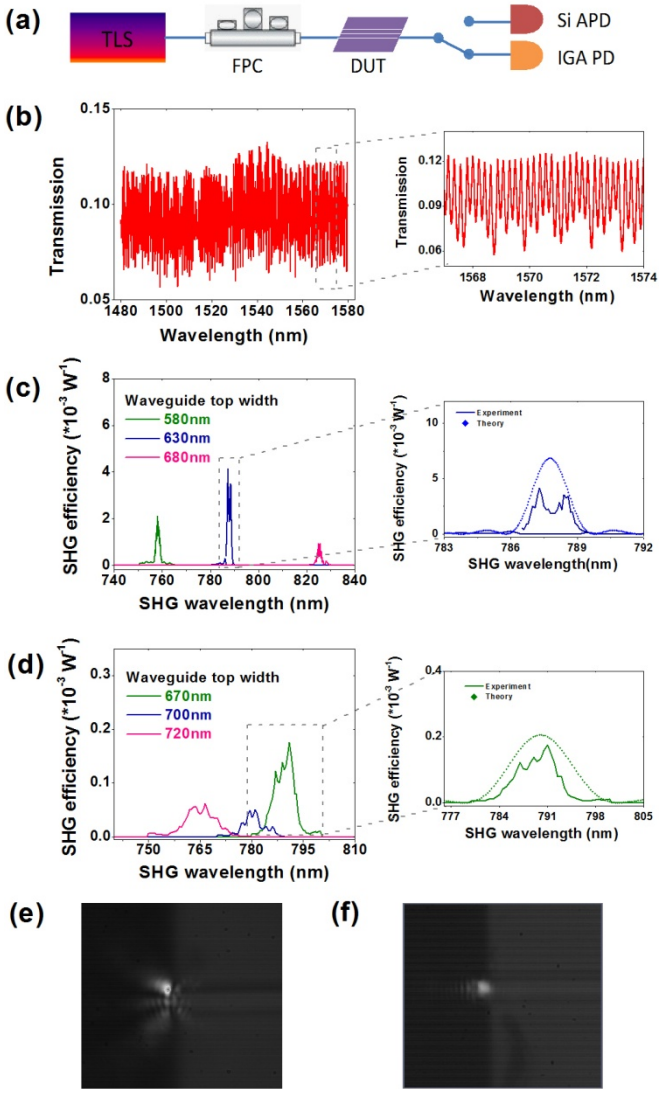

Fig. 4. (a) Schematic of the measurement setup. Light from the telecom tunable laser source (TLS) is coupled into the device under test (DUT) after passing through a fiber polarization controller (FPC). SHG signal is measured using a silicon avalanche photodetector (Si APD), while linear transmission at telecom wavelength is monitored using an InGaAs photodetector (IGA PD). (b) Transmission spectrum of a typical uniform LN waveguide. Inset: zoom-in view of the wavelength range used for calculating propagation loss. (c-d) Conversion efficiency versus SHG wavelength for uniform LN waveguides (c) and PGLN waveguides (d) with different waveguide top widths. Insets: comparison between experimental (solid) and theoretical (dotted) SHG efficiencies and bandwidths. (e-f) CCD camera images of the scattered SHG light at the output facets of a uniform LN waveguide (e) and a PGLN waveguide (f), indicating the corresponding output optical modes.

The dotted curves in the insets of Figs. 4(c) and 4(d) show the theoretical SHG response calculated using the methods described in Section 2. The measured (quasi-) phase matching bandwidths match well with theoretical prediction, while the peak efficiencies are slightly lower than theory, indicating possible inhomogeneity in the waveguide dimensions throughout the chip.

To confirm that the generated SH light couple to third-order and fundamental mode in the case of natural and groove-assisted phase matching, respectively, we used a high NA (0.8) lens and a black & white visible CCD camera to monitor the scattered SH light at the output facet [Figs. 4(e) and 4(f)]. In the case of uniform LN waveguide [Fig. 4(e)], the SHG signal clearly radiates in three lobes, indicating SH light being generated in the 3rd order transverse mode. In comparison, the SH light generated in the PGLN waveguide [Fig. 4(f)] is in the fundamental mode and radiates only in one lobe.

5. CONCLUSIONS

To conclude, we have demonstrated efficient nonlinear wavelength conversion in sub-wavelength LN waveguides, which are realized by a top-down fabrication method and can be densely integrated and mass produced. Our waveguides feature a low propagation loss of 2.52 dB/cm, which is crucial for a practical nonlinear optical system. The lithographically defined nano-structures offer versatile phase matching possibilities for SHG. We have presented both natural phase matching in uniform LN waveguides and quasi-phase matching in PGLN waveguides, achieving normalized conversion efficiencies of 41% $W^{-1}cm^{-2}$ and 7.0% $W^{-1}cm^{-2}$, respectively. These values are on par with PPLN in both ion-exchanged waveguides [9, 11] and recently reported SiN-LNOI hybrid waveguides [31], but are achieved with a single lithographic step, and without the need for periodic domain inversion. While phase-matched LN waveguides feature higher conversion efficiency and are easier to fabricate, PGLN waveguides provide fundamental optical modes at both input and output channels, which is more appealing in many applications.

Further optimization on the etched sidewall roughness, including reflow of the resist, could reduce the propagation loss by at least an order of magnitude [26]. This would allow us to extend the total waveguide length beyond conventional PPLN (~ 10 cm). For PGLN waveguides, optimization on the width modulation profile (e.g. sinusoidal modulation) could possibly reduce the scattering loss. Moreover, both methods could be used in a micro-resonator geometry, which would further boost the conversion efficiency by several orders of magnitude, as is already demonstrated in other materials (e.g. AlN [19]). We believe this work is a crucial step towards on-chip quantum wavelength conversion at the single-photon level. Our nanofabricated LN devices are also promising for applications at short wavelengths (UV-visible) where conventional PPLN approaches become challenging since much smaller poling periods are required.

Funding. National Science Foundation (NSF) (ECCS-1609549); AFOSR MURI on Quantum Memories (FA9550-12-1-0025); National Natural Science Foundation of China (11374289, 61590932); Fundamental Research Funds for the Central Universities of China; National Nanotechnology Infrastructure Network (NNIN) Research Experience for Undergraduates (REU) program.

Acknowledgment. The authors thank Zin Lin for valuable discussions, I-Chun Huang for using his APD. We thank Dr. Hui Hu from NANOLN for helpful discussions. Device fabrication was performed at the Center for Nanoscale Systems (CNS) at Harvard University.

†These authors contributed equally to this work.

REFERENCES

1. W. J. Kozlovsky, C. D. Nabors, and R. L. Byer, "Efficient second harmonic generation of a diode-laser-pumped CW Nd:YAG laser using monolithic MgO:LiNbO3 external resonant cavities," IEEE J. Quantum Electron. **24**, 913-919 (1988).
2. K. L. Vodopyanov, M. M. Fejer, X. Yu, J. S. Harris, Y. S. Lee, W. C. Hurlbut, V. G. Kozlov, D. Bliss, and C. Lynch, "Terahertz-wave generation in quasi-phase-matched GaAs," Appl. Phys. Lett. **89**, 141119 (2006).
3. J. P. Meyn, C. Laue, R. Knappe, R. Wallenstein, and M. M. Fejer, "Fabrication of periodically poled lithium tantalate for UV generation with diode lasers," Appl. Phys. B **73**, 111-114 (2001).
4. A. Vaziri, G. Weihs, and A. Zeilinger, "Experimental Two-Photon, Three-Dimensional Entanglement for Quantum Communication," Phys. Rev. Lett. **89**, 240401 (2002).
5. S. Tanzilli, W. Tittel, M. Halder, O. Alibart, P. Baldi, N. Gisin, and H. Zbinden, "A photonic quantum information interface," Nature **437**, 116-120 (2005).
6. S. Zaske, A. Lenhard, C. A. Keßler, J. Kettler, C. Hepp, C. Arend, R. Albrecht, W. M. Schulz, M. Jetter, P. Michler, and C. Becher, "Visible-to-Telecom Quantum Frequency Conversion of Light from a Single Quantum Emitter," Phys. Rev. Lett. **109**, 147404 (2012).
7. M. M. Fejer and R. L. Byer, "Second-harmonic generation of green light in periodically poled planar lithium niobate waveguide," Electron. Lett. **25**, 174-175 (1989).
8. T. Sugita, K. Mizuuchi, Y. Kitaoka, and K. Yamamoto, "31%-efficient blue second-harmonic generation in a periodically poled MgO:LiNbO3 waveguide by frequency doubling of an AlGaAs laser diode," Opt. Lett. **24**, 1590-1592 (1999).
9. K. R. Parameswaran, R. K. Route, J. R. Kurz, R. V. Roussev, M. M. Fejer, and M. Fujimura, "Highly efficient second-harmonic generation in buried waveguides formed by annealed and reverse proton exchange in periodically poled lithium niobate," Opt. Lett. **27**, 179-181 (2002).
10. R. V. Roussev, C. Langrock, J. R. Kurz, and M. M. Fejer, "Periodically poled lithium niobate waveguide sum-frequency generator for efficient single-photon detection at communication wavelengths," Opt. Lett. **29**, 1518-1520 (2004).
11. L. Ming, C. B. E. Gawith, K. Gallo, M. V. O'Connor, G. D. Emmerson, and P. G. R. Smith, "High conversion efficiency single-pass second harmonic generation in a zinc-diffused periodically poled lithium niobate waveguide," Opt. Express **13**, 4862-4868 (2005).
12. D. N. Nikogosyan, *Nonlinear Optical Crystals: A Complete Survey* (Springer-Science, New York, 2005).
13. Y. N. Korkishko, V. A. Fedorov, T. M. Morozova, F. Caccavale, F. Gonella, and F. Segato, "Reverse proton exchange for buried waveguides in LiNbO3," J. Opt. Soc. Am. A **15**, 1838-1842 (1998).
14. P. Del'Haye, A. Schliesser, O. Arcizet, T. Wilken, R. Holzwarth, and T. J. Kippenberg, "Optical frequency comb generation from a monolithic microresonator," Nature **450**, 1214-1217 (2007).
15. A. C. Turner, M. A. Foster, A. L. Gaeta, and M. Lipson, "Ultra-low power parametric frequency conversion in a silicon microring resonator," Opt. Express **16**, 4881-4887 (2008).
16. J. S. Levy, A. Gondarenko, M. A. Foster, A. C. Turner-Foster, A. L. Gaeta, and M. Lipson, "CMOS-compatible multiple-wavelength oscillator for on-chip optical interconnects," Nat. Photonics **4**, 37-40 (2010).
17. C. Xiong, W. Pernice, K. K. Ryu, C. Schuck, K. Y. Fong, T. Palacios, and H. X. Tang, "Integrated GaN photonic circuits on silicon (100) for second harmonic generation," Opt. Express **19**, 10462-10470 (2011).
18. K. Rivoire, S. Buckley, F. Hatami, and J. Vučković, "Second harmonic generation in GaP photonic crystal waveguides," Appl. Phys. Lett. **98**, 263113 (2011).
19. W. H. P. Pernice, C. Xiong, C. Schuck, and H. X. Tang, "Second harmonic generation in phase matched aluminum nitride waveguides and micro-ring resonators," Appl. Phys. Lett. **100**, 223501 (2012).
20. S. Buckley, M. Radulaski, J. Petykiewicz, K. G. Lagoudakis, J. H. Kang, M. Brongersma, K. Biermann, and J. Vučković, "Second-Harmonic Generation in GaAs Photonic Crystal Cavities in (111)B and (001) Crystal Orientations," ACS Photonics **1**, 516-523 (2014).
21. B. J. M. Hausmann, I. Bulu, V. Venkataraman, P. Deotare, and M. Lončar , "Diamond nonlinear photonics," Nat. Photonics **8**, 369-374 (2014).
22. S. Yamada, B. S. Song, S. Jeon, J. Upham, Y. Tanaka, T. Asano, and S. Noda, "Second-harmonic generation in a silicon-carbide-based photonic crystal nanocavity," Opt. Lett. **39**, 1768-1771 (2014).
23. G. Poberaj, H. Hu, W. Sohler, and P. Günter, "Lithium niobate on insulator (LNOI) for micro-photonic devices," Laser Photonics Rev. **6**, 488-503 (2012).
24. C. Wang, M. J. Burek, Z. Lin, H. A. Atikian, V. Venkataraman, I. C. Huang, P. Stark, and M. Lončar, "Integrated high quality factor lithium niobate microdisk resonators," Opt. Express **22**, 30924-30933 (2014).
25. J. Lin, Y. Xu, Z. Fang, M. Wang, J. Song, N. Wang, L. Qiao, W. Fang, and Y. Cheng, "Fabrication of high-Q lithium niobate microresonators using femtosecond laser micromachining," Sci. Rep. **5**, 8072 (2015).
26. J. Wang, F. Bo, S. Wan, W. Li, F. Gao, J. Li, G. Zhang, and J. Xu, "High-Q lithium niobate microdisk resonators on a chip for efficient electro-optic modulation," Opt. Express **23**, 23072-23078 (2015).
27. A. Guarino, G. Poberaj, D. Rezzonico, R. Degl'Innocenti, and P. Gunter, "Electro-optically tunable microring resonators in lithium niobate," Nat. Photonics **1**, 407-410 (2007).
28. C. Wang, M. J. Burek, Z. Lin, H. A. Atikian, V. Venkataraman, I. C. Huang, P. Stark, and M. Lončar, "Integrated Lithium Niobate Nonlinear Optical Devices," in *CLEO: 2015*, OSA Technical Digest (online) (Optical Society of America, 2015), FW1D.1.
29. S. Diziain, R. Geiss, M. Zilk, F. Schrempel, E. B. Kley, A. Tünnermann, and T. Pertsch, "Second harmonic generation in free-standing lithium niobate photonic crystal L3 cavity," Appl. Phys. Lett. **103**, 051117 (2013).
30. L. Cai, Y. Wang, and H. Hu, "Low-loss waveguides in a single-crystal lithium niobate thin film," Opt. Lett. **40**, 3013-3016 (2015).
31. L. Chang, Y. Li, N. Volet, L. Wang, J. Peters, and J. E. Bowers, "Thin film wavelength converters for photonic integrated circuits," Optica **3**, 531-535 (2016).
32. R. W. Boyd, Nonlinear *optics* (Academic press, Massachusetts, 2003).
33. T. Suhara and H. Nishihara, "Theoretical analysis of waveguide second-harmonic generation phase matched with uniform and chirped gratings," IEEE J. Quantum Electron. **26**, 1265-1276 (1990).
34. R. Regener and W. Sohler, "Loss in low-finesse Ti:LiNbO3 optical waveguide resonators," Appl. Phys. B **36**, 143-147 (1985).